




 Cite this: *RSC Adv.*, 2021, 11, 35147

Fabrication of recyclable reduced graphene oxide/graphitic carbon nitride quantum dot aerogel hybrids with enhanced photocatalytic activity†

 Ping Zhao, Bo Jin, * Jing Yan and Rufang Peng *

Recyclable photocatalysts that can efficiently respond to visible light must be developed for practical application. Herein, three-dimensional (3D) reduced graphene oxide (rGO)/graphitic carbon nitride quantum dot (CNQD) aerogel hybrids for harvesting visible light were synthesized *via* a hydrothermal method. The graphitic CNQDs were not only decorated on but also integrated onto the surface of rGO. The CNQDs produced photogenerated charge under visible light. 3D rGO could serve as an acceptor of the photogenerated electrons and stereoscopically facilitated the charge transfer through aerogel networks owing to its high conductivity. The ciprofloxacin removal ratio of the aerogel hybrids was about 6.1 times higher than that of bulk g-C₃N₄.

Received 24th August 2021

Accepted 15th October 2021

DOI: 10.1039/d1ra06347b

rsc.li/rsc-advances

1. Introduction

Antibiotics, as one of the most widespread pharmaceuticals used in disease prevention and treatment of bacterial infection,¹ are only partially removed by traditional wastewater treatment methods.² They can create serious environmental and health problems, such as the development of antibiotic-resistant bacteria.³ Thus, antibiotics must be completely removed from the environment.⁴ Semiconductor photocatalysis is a promising way to decompose antibiotics⁵ because solar energy is an inexhaustible source of energy and semiconductor photocatalysts are highly efficient, inexpensive, and reusable.

Fluorescent semiconductor quantum dots (QDs) have attracted widespread attention because of their unique electronic properties, tunable optical properties and good stability.⁶ Among QDs, CNQDs hold promise for extensive application in bioimaging,⁷ biosensing,⁸ ion detection,⁹ substance testing,¹⁰ drug delivery,¹¹ biomedical applications,¹² electrocatalysis¹³ and photocatalysis^{14,15} owing to their outstanding optical properties.¹⁶ CNQDs are usually employed as photosensitizers to form nanoheterojunction photocatalytic materials, and are combined with various traditional wide-gap photocatalysts to enhance the efficiency of solar light for photocatalytic performances. Moreover, CNQDs can be coupled with photocatalysts to further extend the spectral responsive range of the photocatalytic system to the near infrared ray region. Several CNQDs-based photocatalyst materials have been developed, such as

CNQDs/TiO₂,^{17,18} CNQDs/Bi₂WO₆,¹⁹ CNQDs/g-C₃N₄,¹⁴ CNQDs/h-BN,²⁰ CNQDs/La₂O₃,²¹ CNQDs/GO-InVO₄,²² and so on. Given that the photogenerated carriers of QDs quickly recombined, there are few reports on the use of QDs as the sole photocatalyst without any scavenger.^{23,24}

3D reduced graphene oxide (rGO) aerogels with a macroscopic block appearance are a perfect candidate for photocatalyst carriers or promoter owing to their high specific surface area, superior electron mobility, high chemical and electrochemical stability.²⁵ Hence, these aerogels can be conveniently recycled from the water. Hybrid macroscopic materials, including TiO₂/rGO,²⁶ g-C₃N₄/rGO,^{27,28} Bi₂WO₆/rGO,²⁹ and BiOBr/rGO,³⁰ are promising materials for photocatalysis. The use of 3D aerogels of CNQDs/rGO-based materials as photocatalysts is nothing new. Hu *et al.*¹⁹ constructed CNQDs/GO-InVO₄ as excellent photocatalysts for NO removal. He *et al.*³¹ developed 3D ternary graphene/CQDs/g-C₃N₄ aerogels for methyl orange removal. However, none of them either intentionally or accidentally synthesized the CNQDs/rGO hybrid as a contrast sample.

Herein, we synthesized 3D aerogel photocatalysts by using CNQDs and rGO *via* a hydrothermal method. We tested the visible light photocatalytic performance of the as-prepared samples toward ciprofloxacin (CIP) and tetracycline (TC). We fabricated an intimate interfacial connection and a highly efficient heterojunction interaction between CNQDs and rGO. rGO supplied photoelectrons favorable for transferring channels, and separating the holes and electrons produced by CNQDs. The photocatalysts exhibited good stability and enhanced the photodegradation of CIP and TC under visible light irradiation. Finally, we proposed a possible photocatalytic mechanism by which these hybrid photocatalysts improve visible light photocatalytic performance.

State Key Laboratory of Environment-friendly Energy Materials, School of Materials Science and Engineering, Southwest University of Science and Technology, Mianyang 621010, Sichuan, P. R. China. E-mail: jinbo0428@163.com; rfpeng2006@163.com

† Electronic supplementary information (ESI) available. See DOI: 10.1039/d1ra06347b



2. Experimental

2.1 Preparation of photocatalysts

GO was obtained by oxidizing crystalline flake graphite powder following a Hummers' method reported elsewhere.³² CNQDs were synthesized *via* a hydrothermal method as previously reported,³³ and the details was shown in ESI.†

rGO/CNQD composite aerogels were synthesized as follows (Scheme 1): different volumes of CNQDs solution was mixed with 10 mL GO (2 mg mL^{-1}) under ultrasonication for a few minutes, and then 80 μL of ethylenediamine was introduced. The mixed suspension was heated at 90 °C for 7 h without stirring to obtain a columnar hydrogel. After lyophilization, the rGO/CNQD 3D aerogel hybrids were obtained. The rGO/CNQD composite aerogels were denoted as rGO/CNQDs- x , where x represents the volume of CNQDs added during the preparation process. Pure graphene aerogels were following the same steps but without the addition of CNQDs.

2.2 Characterization of rGO/CNQDs aerogels

The morphology of the materials were studied *via* field emission scanning electron microscopy (FE-SEM, Hitachi TM4000). High-resolution transmission electron microscopy (HRTEM) images were observed using JEOL JEM 2100F. Crystallographic structure was measured *via* X-ray diffraction (XRD, Philips X' Pert PRO, the Netherlands). The materials were characterized *via* Fourier transform infrared (FT-IR) spectroscopy by using a Spectrum One Autoima spectrometer. Brunauer–Emmett–Teller (BET) surface areas were measured using Micromeritics ASAP2460 system. Composite was analyzed *via* X-ray photoelectron spectroscopy (XPS, Thermo VG 250, USA). The CHI chemical properties of the aerogels were examined *via* photocurrent and electrochemical impedance spectroscopy (EIS). Electron spin resonance (ESR) spectra were recorded using a Bruker EMXnano spectrometers, which detected the signal of $\cdot\text{O}_2^-$; 50 mM 5,5-dimethyl-1-pyrroline *N*-oxide (DMPO) solution was used as the paramagnetic species spin-trap agent (methanol dispersion for $\cdot\text{O}_2^-$ trapping). Photoluminescence (PL) spectra were recorded using an RF-6000 fluorescence spectrophotometer, which detected the signal of 2-hydroxyterephthalic acid with terephthalic acid as the probe molecule.³⁴

2.3 Photocatalytic performance

The photocatalytic activity of the synthesized samples was evaluated using a 300 W xenon lamp (Beijing NBT Technology

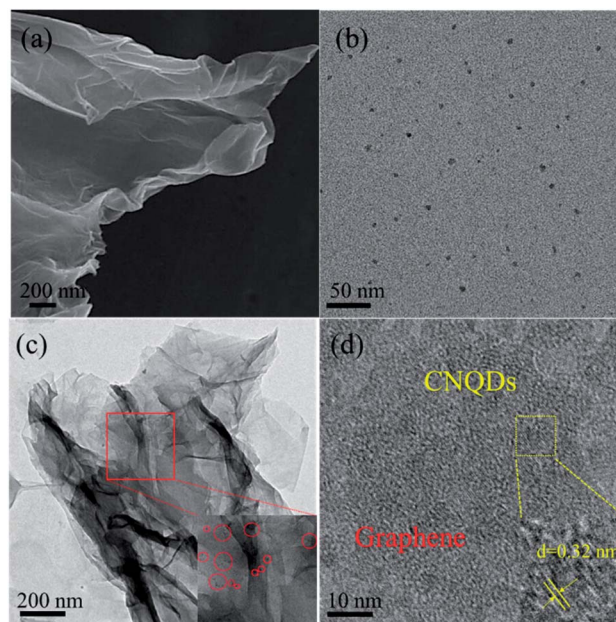


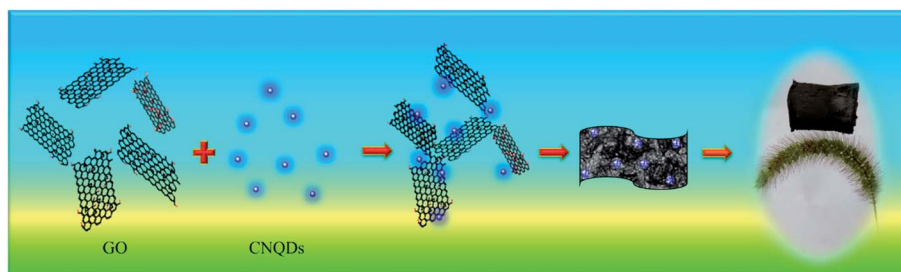
Fig. 1 (a) SEM image of rGO/CNQD-0.02. TEM images of (b) CNQDs and (c) rGO/CNQD-0.02. (d) HTREM images of rGO/CNQD-0.02.

Co., Ltd, China) with a cut-off filter ($\lambda = 420 \text{ nm}$) at ambient temperature. The rGO/CNQDs were used to photodegrade CIP and TC in aqueous solution at a certain concentration. These reaction mixtures were then stirred in the dark for 30 min at room temperature to achieve adsorption equilibrium. At given time intervals, 4.0 mL of the suspension was withdrawn during the photocatalytic process for analysis. The concentrations of CIP and TC were determined by measuring the absorption peak strength at 272 and 355 nm, respectively.

3. Results and discussion

3.1 Morphology and structure of the as-prepared aerogel hybrids

As illustrated in Fig. 1a, the rGO/CNQD-0.02 aerogel hybrid exhibited a two-dimensional laminated structure similar to graphene nanosheets with folds and wrinkles. The TEM image of CNQDs shown in Fig. 1b demonstrated that these quantum dots were evenly dispersed and had a diameter ranging from 2 nm to 6 nm (average diameter of 4.4 nm). In Fig. 1c, the rGO nanosheet remained as a 2D flat and thin structure. This structure are typically formed from only a few layers of graphene



Scheme 1 Schematic of the steps for synthesizing rGO/CNQDs aerogel hybrids.

sheets, and it is helpful for building the 3D model. The CNQDs were loaded on the surfaces of GO, and no aggregation was observed. As shown in Fig. 1d, the CNQDs were loaded on the surface of rGO, and the CNQDs were slightly crystallized. The lattice distance was measured as 0.32 nm in accordance with the (002) plane of $g\text{-C}_3\text{N}_4$.³⁵

As shown in Fig. 2a, in the FT-IR spectra of CNQDs, rGO, and rGO/CNQDs aerogel hybrids, the absorption bands at 3440, 2919, 1633, 1397, and 1048 cm^{-1} were ascribed to the stretching vibrations of O–H, C–H, C=O, and C–N and an antisymmetric stretching of C–O–C,³⁶ respectively. The FT-IR spectra of the aerogel hybrids were evidently similar to those of the main peaks of pure rGO. The result suggested that no obvious structural change in rGO occurred after it combined with the CNQDs, and the CNQDs were successfully incorporated into rGO. The band at 2353 cm^{-1} was ascribed to gaseous CO_2 .³⁷ The crystal structures of graphite, GO, rGO, and rGO/CNQDs aerogel hybrids were examined *via* XRD. Only a sharp diffraction peak appeared at around 10.2° , which corresponded to the (002) reflection for pure GO (Fig. 2b). Moreover, the emergence of the broad peak centered at $2\theta = 24^\circ$ indicated the poor ordering of rGO and hybrids sheets along their stacking directions.³⁸ No clear characteristic diffraction peaks of CNQDs were observed in the aerogel hybrid, and this result could be attributed to the relatively low amount of CNQDs.

On the basis of IUPAC classification, the N_2 adsorption–desorption isotherm of the as-prepared samples was identified as type IV with an H3 type hysteresis loop (Fig. 2c).³⁹ This

isotherm indicated the presence of mesoporous characteristics and slit-like pores in rGO and aerogel hybrids.^{40,41} Barret–Joyner–Halenda analysis revealed that the mesopores in the aerogel hybrids were about 3 nm in diameter (Fig. 2d), which was less than the average diameter of CNQDs (4.4 nm). These micropores completely disappeared compared with those of rGO. The change in pore size distribution plots could be attributed to the fact that the CNQDs were not loaded on the surfaces of rGO. Aside from the π – π stacking and hydrogen-bonding interactions between CNQDs and GO, CNQDs could also be used as a reductant capable of reducing GO (Fig. S1†), resulting in a denser structure.

The CNQDs showed a strong photoluminescence emission peak at 440 nm, whereas the aerogel hybrids exhibited a weak photoluminescence emission peak (Fig. S2†). rGO played an important role in separating the photogenerated carriers generated on the surface of the CNQDs under illumination.

The surface chemical states and the elemental composition of the as-prepared samples were further characterized *via* XPS. The overall XPS spectra showed that C, N, and O elements without other impurities existed in rGO, CNQDs, and the aerogel hybrids (Fig. 3a). The N 1s spectrum of rGO presented two main peaks at 399.1 and 401.0 eV, which could be ascribed to pyridine N and pyrrolic N,⁴² respectively (Fig. 3b). Pyridinic-N, pyrrolic-N, and graphitic-N in the aerogel hybrids were the main components of pristine rGO and CNQDs. Compared with pure rGO, the emergence of pyrrolic N in the aerogel hybrids endowed them with excellent photocatalytic activity.⁴³ Four

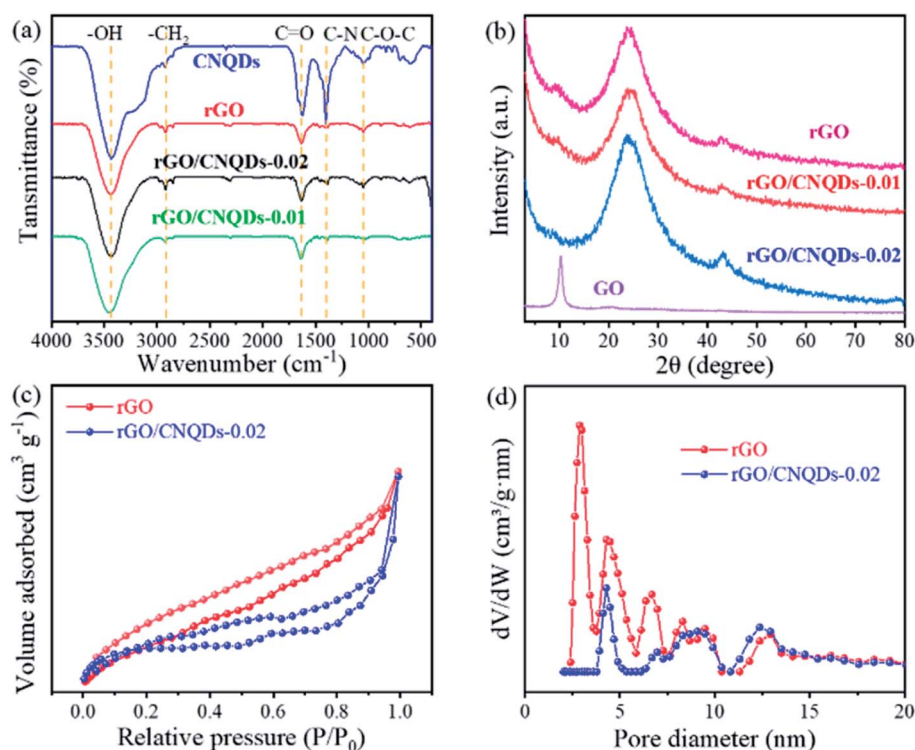


Fig. 2 (a) FT-IR spectra, (b) XRD patterns, (c) nitrogen adsorption–desorption isotherm and (d) the corresponding pore diameter distribution curve of the as-prepared samples.

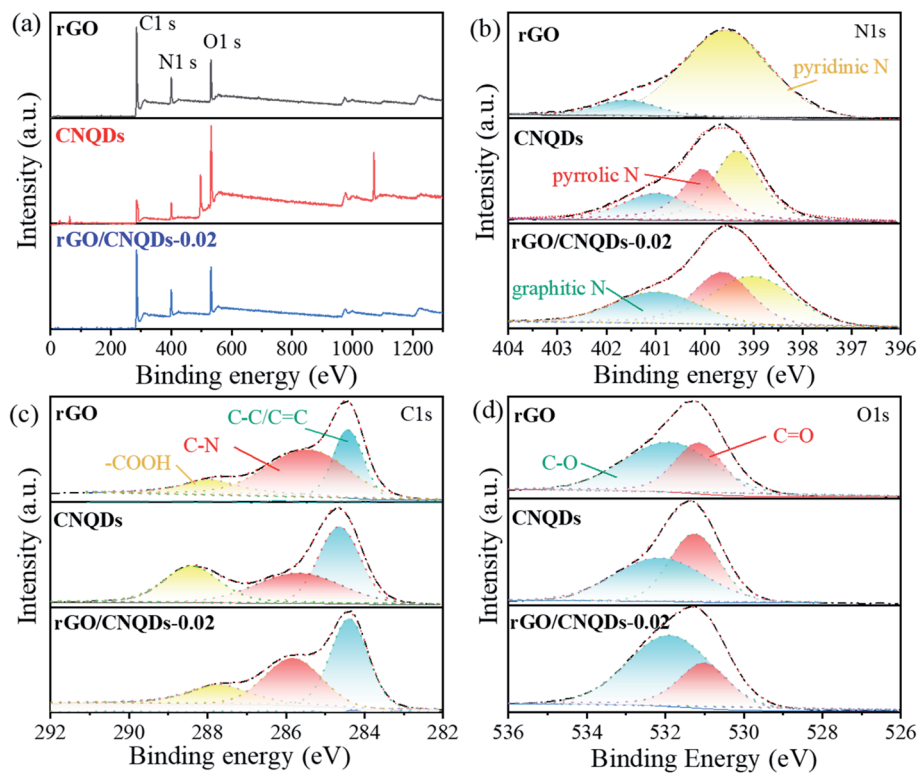


Fig. 3 XPS spectra of pristine CNQDs, rGO, and rGO/CNQDs-0.02: (a) survey. (b) C 1s, (c) N 1s, and (d) O 1s.

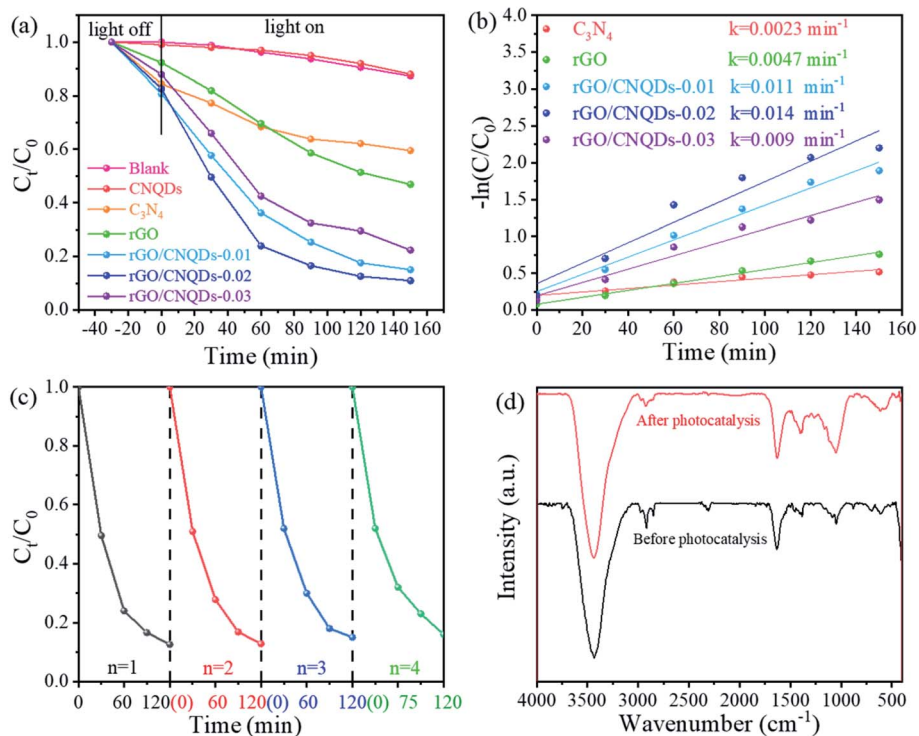


Fig. 4 (a) Visible light photocatalytic removal of aqueous CIP; (b) corresponding first-order kinetic simulation curves and (c) repeated photocatalytic experiments of rGO/CNQDs-0.02 for CIP removal within 4 cycle runs; (d) FT-IR spectra of rGO/CNQDs-0.02 before and after photocatalysis experiments.

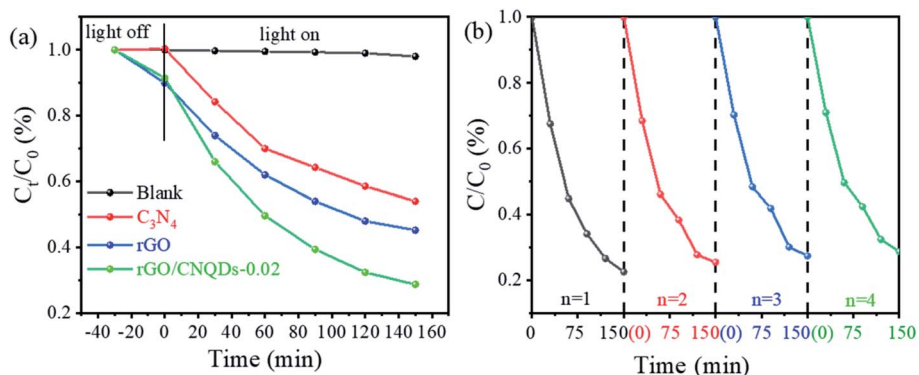


Fig. 5 (a) Photocatalytic degradation of TC by the as-prepared samples under visible light ($\lambda > 420$ nm). (b) Cycle runs of rGO/CNQDs-0.02 for TC removal.

distinct peaks appeared at 284.4, 285.5, and 287.8 eV, which corresponded to C–C/C=C, C–N, and COOH, respectively (Fig. 3c).⁴⁴ The functional groups in the aerogel hybrids were clearly mainly derived from rGO and CNQDs, suggesting that the CNQDs were incorporated well with rGO. The O 1s spectrum showed two binding energies at 532.0 and 531.1 eV, which were assigned to C=O and C–O, respectively (Fig. 3d).

The photocatalytic performance of the as-prepared samples was evaluated by examining the photodegradation of CIP under visible light irradiation. The photodegradation rates of CIP aqueous solution under visible light irradiation without a photocatalyst or with CNQDs could be neglected (Fig. 4a). In 150 min, only 40% and 50% of CIP was removed by $g-C_3N_4$ and rGO, respectively. The visible light photocatalytic activities of the aerogel hybrids were substantially higher than those of pure rGO because of the positive effect of the CNQDs. Among the aerogel hybrids, rGO/CNQDs-0.01 displayed the best adsorption capability, whereas rGO/CNQDs-0.02 exhibited the highest visible light photocatalytic rate, and its reaction rate constant of CIP degradation (0.014 min^{-1}) was about 3.4 and 6.1 times higher than that of rGO and $g-C_3N_4$, respectively (Fig. 4b). Nevertheless, the photocatalytic efficiency of the rGO/CNQDs-0.03 decreased slightly. Due to mesoporous structure,^{45,46} the rGO/CNQDs-0.02 have big surface areas with high catalytic

activity,⁴⁷ but too much CNQDs will result in more density structure for its reducibility, and inhibit the separation of photogenerated electrons and holes.⁴⁸

For further analysis of the photocatalytic reaction products, the CIP solution were filtered and then analyzed by the TOC test. Before and after the visible light irradiation, the TOC content were 27.9 and 9.5 mg L^{-1} respectively, and the TOC removal rate was 65.9%.

The stability of rGO/CNQDs-0.02 was also measured by repeating the photodegradation experiments for four cycles. No considerable loss of photocatalytic activity occurred after four successive cycles, indicating that the aerogel hybrids possessed excellent stability (Fig. 4c). A comparison of the FTIR patterns of the rGO/CNQDs-0.02 aerogel hybrid before and after the four cycles of photocatalytic experiments did not reveal any change, implying that the aerogel hybrids possessed excellent reusability and stability without structural degradation during the photocatalytic reaction process (Fig. 4d).

The catalytic properties of rGO/CNQDs-0.02 as a response to visible light were further evaluated by testing the photodegradation of TC under visible light. The self-degradation of TC within 150 min under visible light irradiation was negligible (Fig. 5a). The hybrid catalysts exhibited excellent visible light activity compared with the pristine rGO and $g-C_3N_4$. These

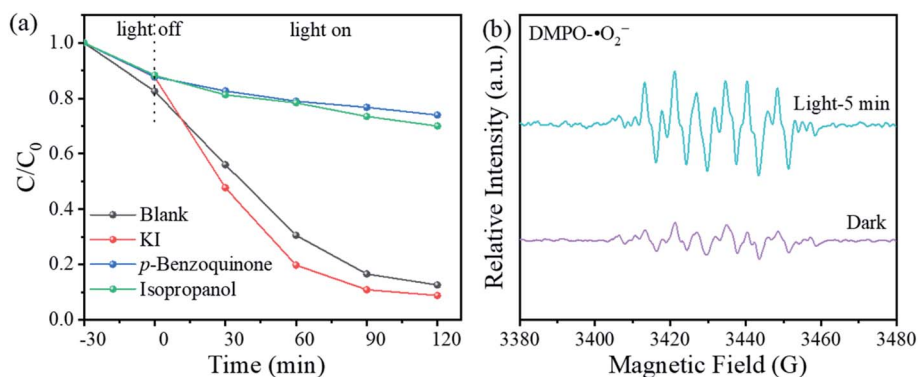


Fig. 6 (a) Effects of scavengers on the photocatalytic degradation of CIP with rGO/CNQDs-0.02 under visible light irradiation; (b) ESR spectra of DMPO- $\cdot O_2^-$ adducts.

results were consistent with those on CIP degradation. The photodegradation efficiencies of TC also exhibited no remarkable reduction after four successive cycles (Fig. 5b).

The role of the main reactive species involved in photocatalytic degradation in the presence of rGO/CNQDs-0.02 was examined *via* trapping tests (Fig. 6a). KI, isopropanol, and *p*-benzoquinone were adopted as the scavengers of hole (h^+), hydroxyl radical ($\cdot\text{OH}$), and super oxide radical ($\cdot\text{O}_2^-$).⁴⁹ The introduction of KI into the CIP aqueous solution further enhanced the photodegradation efficiency (Fig. 6a). By contrast, isopropanol and *p*-benzoquinone inhibited the photodegradation efficiency, indicating that $\cdot\text{OH}$ and $\cdot\text{O}_2^-$ were the main reactive species in photocatalytic process of rGO/CNQDs-0.02.

The roles of the $\cdot\text{O}_2^-$ in this photocatalysis process was determined further *via* the ESR. The weak signal of $\cdot\text{O}_2^-$ was detected in the dark probably because and sample was not protected from light before the test was conducted (Fig. 6b). Under illumination, the obvious signal of DMPO- $\cdot\text{O}_2^-$ could be observed.

The $\cdot\text{OH}$ can readily react with terephthalic acid in basic solution to generate 2-hydroxyterephthalic acid which emits a unique fluorescence signal centered at about 420 ± 6 nm under excitation at 315 nm. Moreover, the PL intensity of 2-hydroxyterephthalic acid is proportional to the amount of $\cdot\text{OH}$.²² The PL peak centered at about 420 nm obviously increased with the extension of irradiation time in the presence of the aerogel hybrids (Fig. S3†). This result implied that $\cdot\text{OH}$ radicals were actually generated under visible light irradiation, and fluorescent intensity increased with irradiation time.

The results of scavenger test, ESR, and PL confirmed that $\cdot\text{O}_2^-$ and $\cdot\text{OH}$ existed in the rGO/CNQDs-0.02 system under visible light irradiation.

The photoinduced charge transfer and separation behaviors were confirmed *via* electrochemical experiments. EIS revealed that the aerogel hybrids had a small diameter of semicircular Nyquist curve, indicating that electronic impedance was reduced and mobility was improved (Fig. 7a).⁵⁰ As a zero-band-gap semiconductor, rGO is electrically conductive with a low photocurrent density. The aerogel hybrids had a strengthened photocurrent transient photocurrent response, and photocurrent density improved by about 2 times higher than that of $g\text{-C}_3\text{N}_4$ (Fig. 7b).

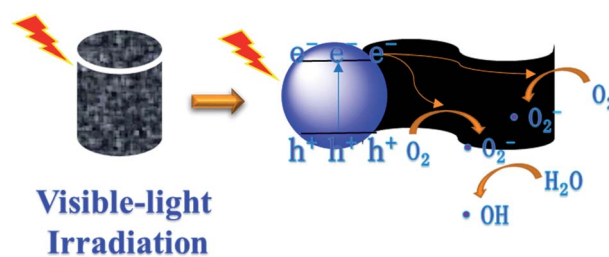


Fig. 8 Schematic of the mechanisms of photodegradation processes in the presence of the aerogel hybrids under visible-light irradiation.

On the basis of these results, the mechanism of photodegradation of rGO/CNQDs-0.02 under visible light irradiation was proposed (Fig. 8). When the aerogel hybrids are irradiated under visible light, the CNQDs generated electrons, which are transferred into the valence band of the CNQDs and then rapidly transferred by rGO to avoid the recombination of photo-generated electron-hole pairs.⁵¹ Finally, the electrons on the surface of GO capture the adsorbed O_2 on the composite catalyst surface and reduce it to $\cdot\text{O}_2^-$ radicals to further degrade CIP. Given that the VB holes of $g\text{-C}_3\text{N}_4$ are more positive than the energy level of OH^- or H_2O , $g\text{-C}_3\text{N}_4$ cannot directly oxidized $\text{OH}^-/\text{H}_2\text{O}$ into $\cdot\text{OH}$ radicals.⁵² Therefore, $\cdot\text{OH}$ may be generated by $\cdot\text{O}_2^-$ radicals that are partially oxidizing H_2O .

4. Conclusions

In conclusion, we successfully fabricated a convenient and recyclable 3D rGO/CNQD aerogel *via* a facile hydrothermal process. We investigated its photocatalytic properties for degradation of CIP and TC under visible light. The CNQDs produced photoelectrons and holes under visible light, and they could be effectively separated by rGO because of its exceptionally high conductivity. The photodegradation for CIP and TC under visible light demonstrated the excellent performance of the as-prepared aerogel hybrids. The photocatalytic performance of the aerogel hybrids in CIP and TC degradation was slightly reduced after four runs. Results of scavenger tests, PL tests, and ESR revealed that the active species $\cdot\text{O}_2^-$ and $\cdot\text{OH}$ were produced in the photocatalyst system. This work provides new insight into the designing of CNQD-based heterostructural

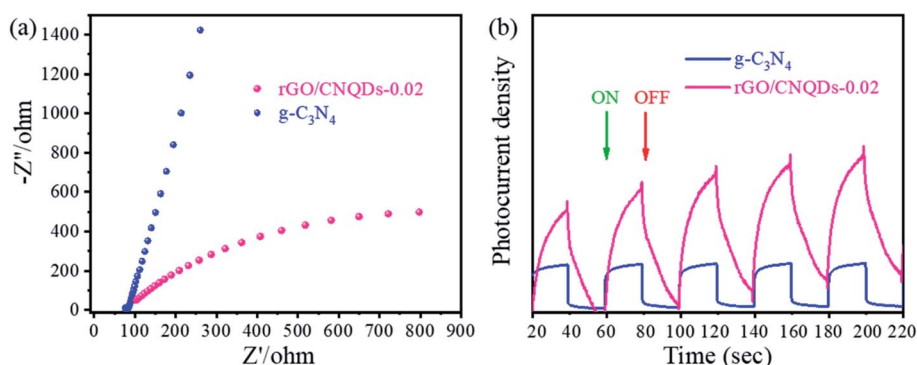


Fig. 7 (a) EIS, and (b) transient photocurrent response of rGO/CNQDs-0.02 and $g\text{-C}_3\text{N}_4$.

photocatalysts with an effective charge separation and CNQDs as an excellent semiconductor.

Conflicts of interest

There are no conflicts to declare.

Acknowledgements

This work was carried out with the financial support received from the Natural Science Foundation of China (51972278), Outstanding Youth Science and Technology Talents Program of Sichuan (19JCQN0085), and Open Project of State Key Laboratory of Environment-friendly Energy Materials (20fksy16).

References

- 1 E. S. Elmolla and M. Chaudhuri, Photocatalytic degradation of amoxicillin, ampicillin and cloxacillin antibiotics in aqueous solution using UV/TiO₂ and UV/H₂O₂/TiO₂ photocatalysis, *Desalination*, 2010, **252**, 46–52.
- 2 D. Kanakaraju, J. Kockler, C. A. Motti, B. D. Glass and M. Oelgemöller, Titanium dioxide/zeolite integrated photocatalytic adsorbents for the degradation of amoxicillin, *Appl. Catal., B*, 2015, **166–167**, 45–55.
- 3 D. Klauson, J. Babkina, K. Stepanova, M. Krichevskaya and S. Preis, Aqueous photocatalytic oxidation of amoxicillin, *Catal. Today*, 2010, **151**, 39–45.
- 4 Y. C. Deng, L. Tang, C. Y. Feng, G. M. Zeng, J. J. Wang, Y. Y. Zhou, Y. N. Liu, B. Peng and H. P. Feng, Construction of plasmonic Ag modified phosphorous-doped ultrathin g-C₃N₄ nanosheets/BiVO₄ photocatalyst with enhanced visible-near-infrared response ability for ciprofloxacin degradation, *J. Hazard. Mater.*, 2018, **344**, 758–769.
- 5 K. Wang, G. K. Zhang, J. Li, Y. Li and X. Y. Wu, 0D/2D Z-scheme heterojunctions of bismuth tantalate quantum dots/ultrathin g-C₃N₄ nanosheets for highly efficient visible light photocatalytic degradation of antibiotics, *ACS Appl. Mater. Interfaces*, 2017, **9**(50), 43704–43715.
- 6 T. Wang, C. Y. Nie, Z. M. Ao, S. B. Wang and T. C. An, Recent progress in g-C₃N₄ quantum dots: synthesis, properties and applications in photocatalytic degradation of organic pollutants, *J. Mater. Chem. A*, 2020, **8**, 485–502.
- 7 Y. C. Lu, J. Chen, A. J. Wang, N. Bao, J. J. Feng, W. P. Wang and L. X. Shao, Facile synthesis of oxygen and sulfur co-doped graphitic carbon nitride fluorescent quantum dots and their application for mercury (II) detection and bioimaging, *J. Mater. Chem. C*, 2015, **3**, 73–78.
- 8 Q. J. Lu, H. Y. Wang, Y. L. Liu, Y. X. Hou, H. T. Li and Y. Y. Zhang, Graphitic carbon nitride nanodots: as reductant for the synthesis of silver nanoparticles and its biothiols biosensing application, *Biosens. Bioelectron.*, 2017, **89**, 411–416.
- 9 Z. X. Zhou, Y. F. Shen, Y. Li, A. Liu, S. Q. Liu and Y. J. Zhang, Chemical cleavage of layered carbon nitride with enhanced photoluminescent performances and photoconduction, *ACS Nano*, 2015, **9**(12), 12480–12487.
- 10 Y. L. Thi Ngou, J. S. Chung and S. H. Hur, Aminoboronic acid-functionalized graphitic carbon nitride quantum dots for the photoluminescence multi-chemical sensing probe, *Dyes Pigm.*, 2019, **168**, 180–188.
- 11 L. S. Lin, Z. X. Cong, J. Li, K. M. Ke, S. S. Guo, H. H. Yang and G. N. Chen, Graphitic-phase C₃N₄ nanosheets as efficient photosensitizers and pH-responsive drug nanocarriers for cancer imaging and therapy, *J. Mater. Chem. B*, 2014, **2**(8), 1031–1037.
- 12 G. F. Liao, F. He, Q. Li, L. Zhong, R. Z. Zhao, H. N. Che, H. Y. Gao and B. Z. Fang, Emerging graphitic carbon nitride-based materials for biomedical applications, *Prog. Mater. Sci.*, 2020, **112**, 100666.
- 13 B. Z. Fang, I. Daniel, A. Bonakdarpour, R. Govindarajan, J. Sharman and D. P. Wilkinson, Dense Pt nanowire electrocatalyst for improved fuel cell performance using a graphitic carbon nitride-decorated hierarchical nanocarbon support, *Small*, 2021, **17**, 202102288.
- 14 S. B. Wang, X. Han, Y. H. Zhang, N. Tian, T. Y. Ma and H. W. Huang, Inside-and-out semiconductor engineering for CO₂ photoreduction: from recent advances to new trends, *Small Struct.*, 2021, **2**(1), 2000061.
- 15 Y. P. Liu, S. J. Shen, Z. G. Li, D. D. Ma, G. Xu and B. Z. Fang, Mesoporous g-C₃N₄ nanosheets with improved photocatalytic performance for hydrogen evolution, *Mater. Charact.*, 2021, **174**, 111031.
- 16 H. J. Liu, X. Y. Wang, H. Wang and R. R. Nie, Synthesis and biomedical applications of graphitic carbon nitride quantum dots, *J. Mater. Chem. B*, 2019, **7**, 5432–5448.
- 17 Y. H. Li, K. L. Lv, W. K. Ho, F. Dong, X. F. Wu and Y. Xia, Hybridization of rutile TiO₂ (rTiO₂) with g-C₃N₄ quantum dots (CNQDs): An efficient visible-light-driven Z-scheme hybridized photocatalyst, *Appl. Catal., B*, 2017, **202**, 611–619.
- 18 R. B. Guo, D. D. Zeng, Y. Xie, Y. Ling, D. Zhou, L. S. Jiang, W. Y. Jiao, J. S. Zhao and S. Q. Li, Carbon nitride quantum dots (CNQDs)/TiO₂ nanoparticle heterojunction photocatalysts for enhanced ultraviolet-visible-light-driven bisphenol A degradation and H₂ production, *Int. J. Hydrogen Energy*, 2020, **45**(43), 22534–22544.
- 19 M. J. Zhang, Y. Zhang, L. Tang, G. M. Zeng, J. J. Wang, Y. Zhu, C. Y. Feng, Y. C. Deng and W. Z. He, Ultrathin Bi₂WO₆ nanosheets loads g-C₃N₄ quantum dots: A direct Z-scheme photocatalyst with enhanced photocatalytic activity towards degradation of organic pollutants under wide spectrum light irradiation, *J. Colloid Interface Sci.*, 2019, **539**, 654–664.
- 20 T. Wang, X. Q. Liu, Q. Y. Men, C. C. Ma, Y. Liu, Z. Liu, P. W. Huo, C. X. Li and Y. S. Yan, Green synthesis g-C₃N₄ quantum dots loading h-BN for efficient and stable photocatalytic performance, *J. Mol. Liq.*, 2018, **268**, 561–568.
- 21 Y. Xie, J. Wu, C. Y. Sun, Y. Ling, S. Q. Li, X. Li, X. Li, J. S. Zhao and K. Yang, La₂O₃-modified graphite carbon nitride achieving the enhanced photocatalytic degradation of different organic pollutants under visible light irradiation, *Mater. Chem. Phys.*, 2020, **246**, 122846.
- 22 J. D. Hu, D. Y. Chen, N. J. Li, Q. F. Xu, H. Li, J. H. He and J. M. Lu, Fabrication of graphitic-C₃N₄ quantum dots/

- graphene-InVO₄ aerogel hybrids with enhanced photocatalytic NO removal under visible-light irradiation, *Appl. Catal., B*, 2018, **236**, 45–52.
- 23 S. L. Hu, R. X. Tian, Y. G. Dong, J. L. Yang, J. Liu and Q. Chang, Modulation and effects of surface groups on photoluminescence and photocatalytic activity of carbon dots, *Nanoscale*, 2013, **5**, 11665–11671.
- 24 S. Y. Lim, W. Shen and Z. Q. Gao, Carbon quantum dots and their applications, *Chem. Soc. Rev.*, 2015, **44**, 362–381.
- 25 N. Zhang, Y. H. Zhang and Y. J. Xu, Recent progress on graphene-based photocatalysts: current status and future perspectives, *Nanoscale*, 2012, **4**, 5792–5813.
- 26 M. Nawaz, W. Miran, J. Jang and D. S. Lee, One-step hydrothermal synthesis of porous 3D reduced graphene oxide/TiO₂ aerogel for carbamazepine photodegradation in aqueous solution, *Appl. Catal., B*, 2017, **203**, 85–95.
- 27 L. Tang, C. T. Jia, Y. C. Xue, L. Li, A. Q. Wang, G. Xu, N. Liu and M. H. Wu, Fabrication of compressible and recyclable macroscopic g-C₃N₄/GO aerogel hybrids for visible-light harvesting: A promising strategy for water remediation, *Appl. Catal., B*, 2017, **219**, 241–248.
- 28 W. C. Wan, S. Yu, F. Dong, Q. Zhang and Y. Zhou, Efficient C₃N₄/graphene oxide aerogel macroscopic visible-light photocatalyst, *J. Mater. Chem. A*, 2016, **4**, 7823–7829.
- 29 T. Chen, L. Z. Liu, C. Hu and H. W. Huang, Recent advances on Bi₂WO₆-based photocatalysts for environmental and energy applications, *Chin. J. Catal.*, 2011, **42**, 1413–1438.
- 30 X. Yu, J. J. Shi, L. J. Feng, C. H. Li and L. Wang, A three-dimensional BiOBr/RGO heterostructural aerogel with enhanced and selective photocatalytic properties under visible light, *Appl. Surf. Sci.*, 2017, **396**, 1775–1782.
- 31 H. J. He, L. H. Huang, Z. J. Zhong and S. Z. Tan, Constructing three-dimensional porous graphene-carbon quantum dots/g-C₃N₄ nanosheet aerogel metal-free photocatalyst with enhanced photocatalytic activity, *Appl. Surf. Sci.*, 2018, **441**, 285–294.
- 32 J. Chen, B. Yao, C. Li and G. Q. Shi, An improved Hummers method for eco-friendly synthesis of graphene oxide, *Carbon*, 2013, **64**, 225–229.
- 33 P. Zhao, B. Ji, Q. C. Zhang and R. F. Peng, High-quality carbon nitride quantum dots on photoluminescence: effect of carbon sources, *Langmuir*, 2021, **37**(5), 1760–1767.
- 34 T. Hirakawa and Y. Nosaka, Properties of O₂^{•-} and OH[•] formed in TiO₂ aqueous suspensions by photocatalytic reaction and the influence of H₂O₂ and some ions, *Langmuir*, 2002, **18**, 3247–3254.
- 35 W. J. Ong, L. Tan, S. P. Chai and S. T. Yong, Graphene oxide as a structure-directing agent for the two-dimensional interface engineering of sandwich-like graphene/g-C₃N₄ hybrid nanostructures with enhanced visible-light photoreduction of CO₂ to methane, *Chem. Commun.*, 2015, **51**, 858–861.
- 36 S. J. Zhu, Q. N. Meng, L. Wang, J. H. Zhang, Y. B. Song, H. Jin, K. Zhang, H. C. Sun, H. Y. Wang and B. Yang, Highly photoluminescent carbon dots for multicolor patterning, sensors, and bioimaging, *Angew. Chem., Int. Ed.*, 2013, **125**(14), 4045–4049.
- 37 L. F. Liao, C. F. Lien, D. L. Shieh, F. C. Chen and J. L. Lin, FTIR study of adsorption and photochemistry of amide on powdered TiO₂: Comparison of benzamide with acetamide, *Phys. Chem. Chem. Phys.*, 2002, **4**, 4584–4589.
- 38 Y. Q. Sun, Q. Wu and G. Q. Shi, Supercapacitors based on self-assembled graphene organogel, *Phys. Chem. Chem. Phys.*, 2011, **13**, 17249–17254.
- 39 Y. L. Xing, B. Z. Fang, A. Bonakdarpour, S. C. Zhang and D. P. Wilkinson, Facile fabrication of mesoporous carbon nanofibers with unique hierarchical nanoarchitecture for electrochemical hydrogen storage, *Int. J. Hydrogen Energy*, 2014, **39**, 7859–7867.
- 40 B. Z. Fang, A. Bonakdarpour, K. Reilly, Y. L. Xing, F. Taghipour and D. P. Wilkinson, Large-scale synthesis of TiO₂ microspheres with hierarchical nanostructure for highly efficient photo driven reduction of CO₂ to CH₄, *ACS Appl. Mater. Interfaces*, 2014, **6**, 15488–15498.
- 41 B. Z. Fang, Y. L. Xing, A. Bonakdarpour, S. C. Zhang and D. P. Wilkinson, Hierarchical CuO-TiO₂ hollow microspheres for highly efficient photodriven reduction of CO₂ to CH₄, *ACS Sustainable Chem. Eng.*, 2015, **3**, 2381–2388.
- 42 D. Vashishit, E. Sharma, M. Kaur, A. Vashisht, S. K. Metha and K. Singh, Solvothermal assisted phosphate functionalized graphitic carbon nitride quantum dots for optical sensing of Fe ions and its thermodynamic aspects, *Spectrochim. Acta, Part A*, 2020, **228**, 117773.
- 43 S. Bhattacharyya, F. Ehrat, P. Urban, R. Teves, R. Wyrwich, M. Doblinger, J. Feldmann, A. S. Urban and J. K. Stolarczyk, Effect of nitrogen atom positioning on the trade-off between emissive and photocatalytic properties of carbon dots, *Nat. Commun.*, 2017, **8**, 1401.
- 44 Q. Zhang, Y. Y. Liu, Y. X. Nie, Y. Liu and Q. Ma, Wavelength-dependent surface plasmon coupling electrochemiluminescence biosensor based on sulfur doped carbon nitride quantum dots for K-RAS gene detection, *Anal. Chem.*, 2019, **91**(21), 13780–13786.
- 45 B. Z. Fang, M. Kim, J. H. Kim and J. S. Yu, Controllable synthesis of hierarchical nanostructured hollow core/mesopore shell carbon for electrochemical hydrogen storage, *Langmuir*, 2008, **24**, 12068–12072.
- 46 Y. J. Wang, B. Z. Fang, H. Li, X. T. Bi and H. J. Wang, Progress in modified carbon support materials for Pt and Pt-alloy cathode catalysts in polymer electrolyte membrane fuel cells, *Prog. Mater. Sci.*, 2016, **82**, 445–498.
- 47 B. Z. Fang, S. Q. Fan, J. H. Kim, M. S. Kim, M. Kim, N. K. Chaudhari, J. Ko and J. S. Yu, Incorporating hierarchical nanostructured carbon counter electrode into metal-free organic dye-sensitized solar cell, *Langmuir*, 2010, **26**(13), 11238–11243.
- 48 R. B. Guo, D. D. Zeng, Y. Xie, Y. Ling, D. Zhou, L. S. Jiang, W. Y. Jiao, J. S. Zhao and S. Q. Li, Carbon nitride quantum dots (CNQDs)/TiO₂ nanoparticle heterojunction photocatalysts for enhanced ultraviolet-visible-light-driven bisphenol a degradation and H₂ production, *Int. J. Hydrogen Energy*, 2020, **45**, 22534–22544.
- 49 C. J. Wang, J. Shen, R. G. Chen, F. Cao and B. Jin, Self-assembled BiOCl/Ti₃C₂T_x composites with efficient photo-

- induced charge separation activity for photocatalytic degradation of p-nitrophenol, *Appl. Surf. Sci.*, 2020, **519**, 146175.
- 50 G. G. Zhang and X. C. Wang, A facile synthesis of covalent carbon nitride photocatalysts by co-polymerization of urea and phenylurea for hydrogen evolution, *J. Catal.*, 2013, **307**, 246–253.
- 51 C. Y. Sun, Q. H. Xu, Y. Xie, Y. Ling, J. I. Jiao, H. H. Zhu, J. S. Zhao, X. M. Liu, B. Hu and D. Zhou, High-efficient one-pot synthesis of carbon quantum dots decorating Bi₂MoO₆ nanosheets heterostructure with enhanced visible-light photocatalytic properties, *J. Alloys Compd.*, 2017, **723**, 333–344.
- 52 A. Nikokavoura and C. Trapalis, Graphene and g-C₃N₄ based photocatalyst for NO_x removal: A review, *Appl. Surf. Sci.*, 2018, **430**, 18–52.